Supplementary Information

Hydrophobic Low-Polarity Perfluorobutanesulfonate Shield Enables Dendrite-Free Aqueous Zn-Ion Batteries

Jiazhi Geng[a], Xiaolang Liu[a], Runming Tao[b], Gaoxu Huang[a], Yuxi Yang[a], Haifeng Li[a], Deyu Wang[a], Zhihong Liu[a] and Jiyuan Liang*[a]

a. Key Laboratory of Flexible Optoelectronic Materials and Technology, Ministry of Education, School of Optoelectronic Materials & Technology, Jianghan University, Wuhan, 430056, Hubei, China. E-mail: liangjy@jhun.edu.cn

b. Independent Researcher, Darien, IL, 60561, USA

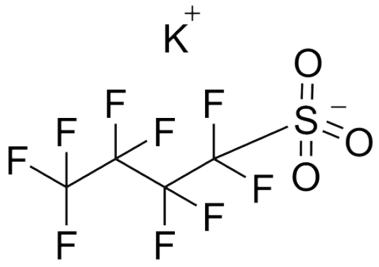

Figure S1. Structural formula of potassium perfluorobutanesulfonate.

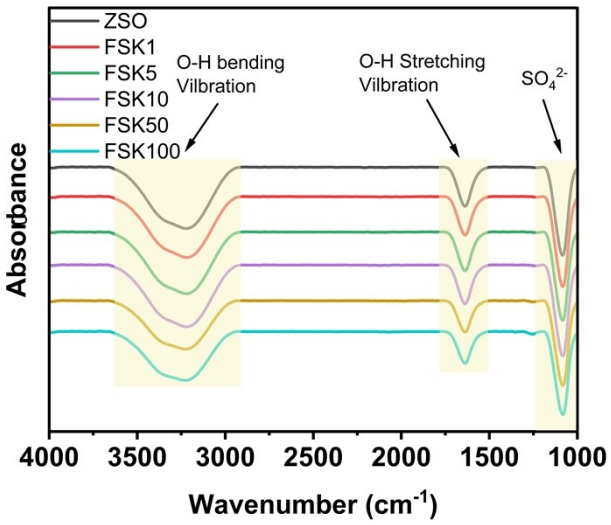

Figure S2. FTIR spectra of various electrolytes.

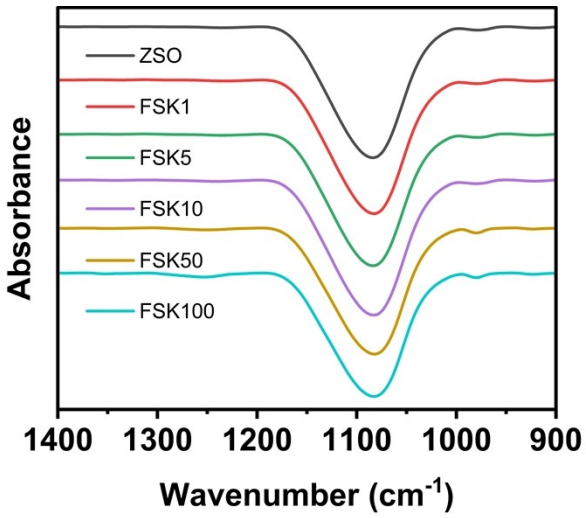

Figure S3. FTIR spectra of $\nu(SO_4^{2-})$ in various electrolytes.

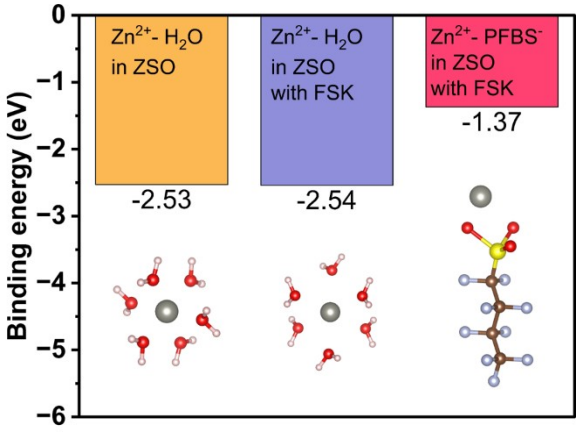

Figure S4. Binding energies of Zn^{2+}-H_2O in ZSO, Zn^{2+}-H_2O in ZSO with FSK, and Zn^{2+}-Perfluorobutanesulfonate ($PFBS^-$) in ZSO with FSK.

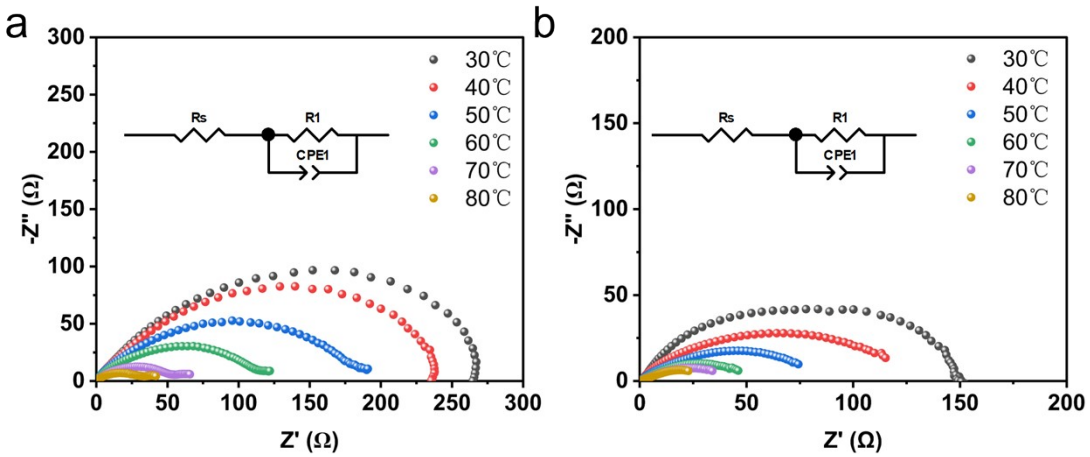

Figure S5. Nyquist plots of the Zn||Zn symmetric cell at various temperatures (a) in ZSO electrolyte and (b) in FSK50 electrolyte.

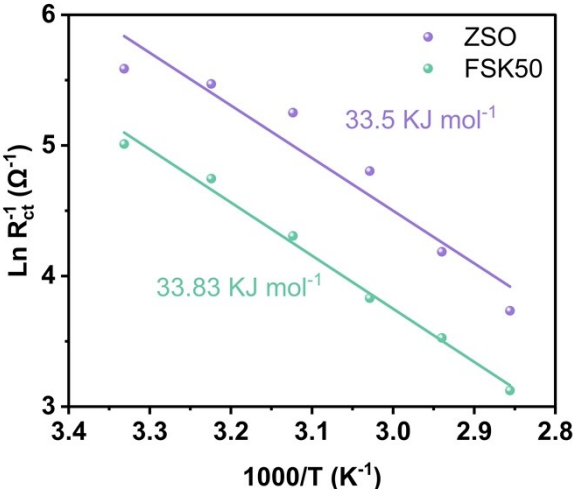

Figure S6. Arrhenius curves and comparison of activation energies.

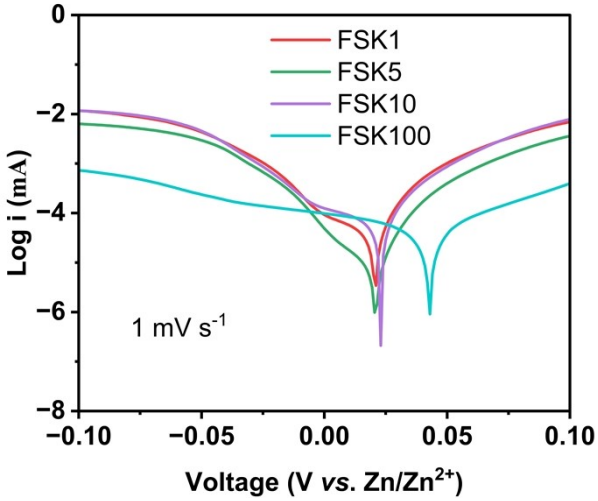

Figure S7. Tafel plots of the Zn electrode in FSK1, FSK5, FSK10 and FSK100 at 1 mV s^{-1} using Zn||Zn symmetrical cells.

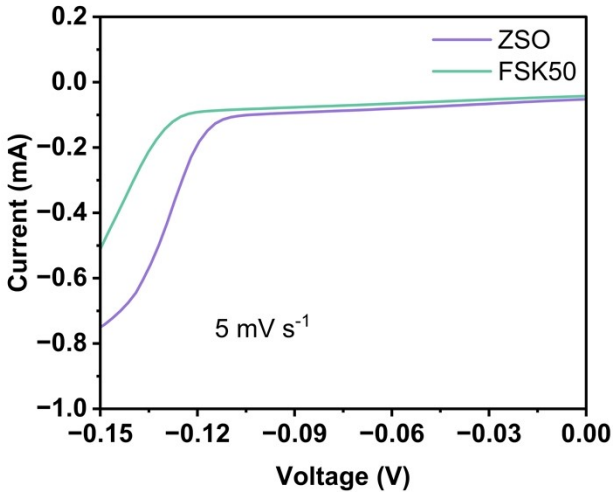

Figure S8. Linear sweep voltammetry (LSV) curves at 5 mV s^{-1} in the Na_2SO_4 electrolytes with/without FSK.

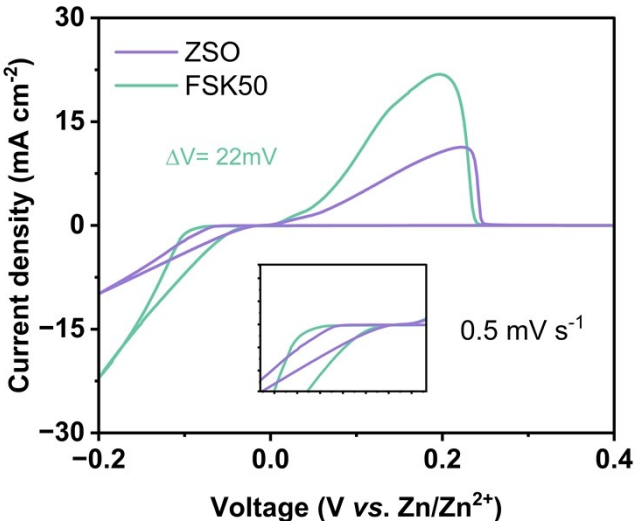

Figure S9. CV curves for Zn||Cu cells at 0.5 mV s^{-1}.

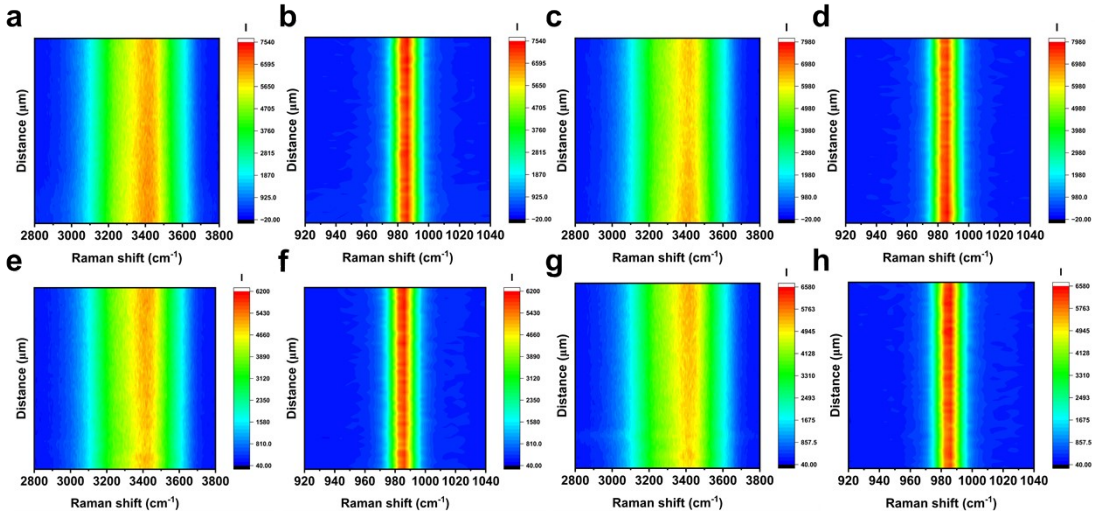

Figure S10. In situ Raman spectra of ZSO at 5 mA cm^{-2} and 10 mAh cm^{-2}: (a) ν(OH), (b) $\nu(SO_4^{2-})$, under open-circuit conditions: (c) ν(OH), (d) $\nu(SO_4^{2-})$. In situ Raman spectra of FSK at 5 mA cm^{-2} and 10 mAh cm^{-2}: (e) ν(OH), (f) $\nu(SO_4^{2-})$, under open-circuit conditions: (g) ν(OH), (h) $\nu(SO_4^{2-})$.

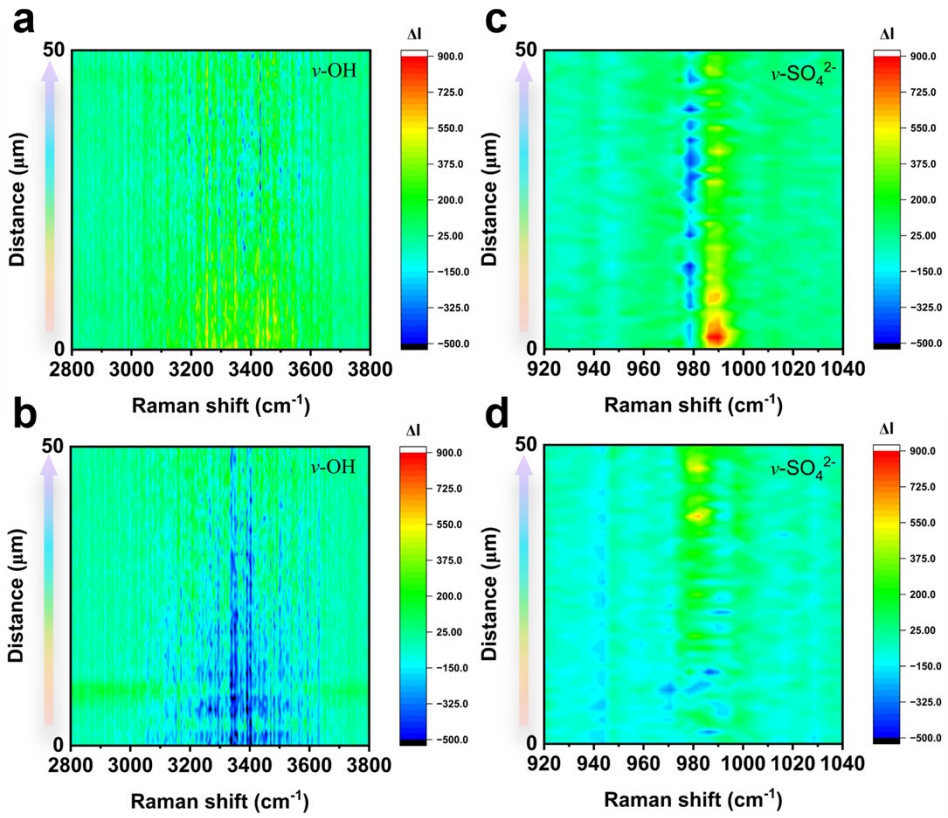

Figure S11. In situ Raman difference spectra of *ν*(OH) at the electrode/electrolyte interface under open-circuit conditions: (a) ZSO electrolyte, (b) FSK50 electrolyte; *ν*(SO_4^{2-}): (c) ZSO electrolyte, (d) FSK50 electrolyte.

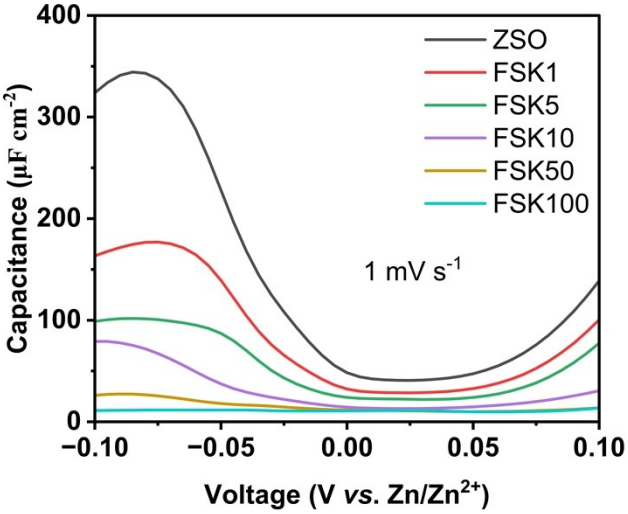

Figure S12. Differential capacity curves of Zn||Zn symmetric cells at the scan rate of 1 mV s^{-1} in various

electrolyte.

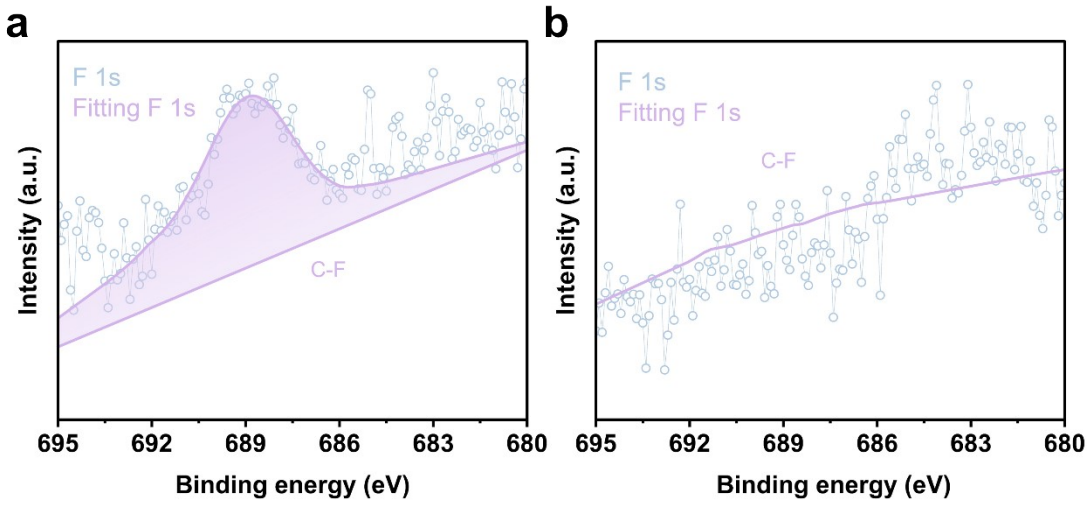

Figure S13. HRXPS spectra of F 1s for Zn anode in (a) FSK50 and (b) ZSO.

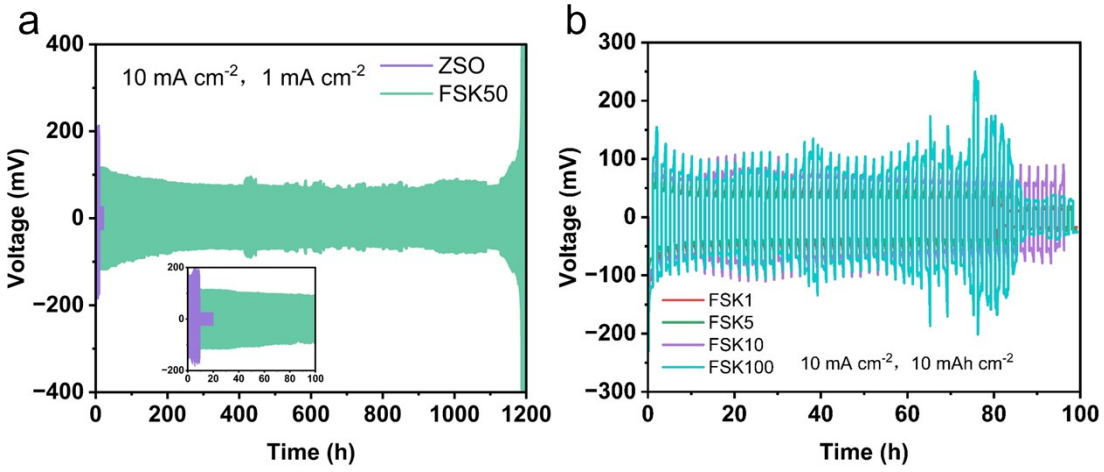

Figure S14. The cycling performance the Zn||Zn symmetrical cell (a) in ZSO and FSK50 at 10 mA cm^{-2} and 1 mAh cm^{-2}, (b) in FSK1, FSK5, FSK10 and FSK100 at 10 mA cm^{-2} and 10 mAh cm^{-2}.

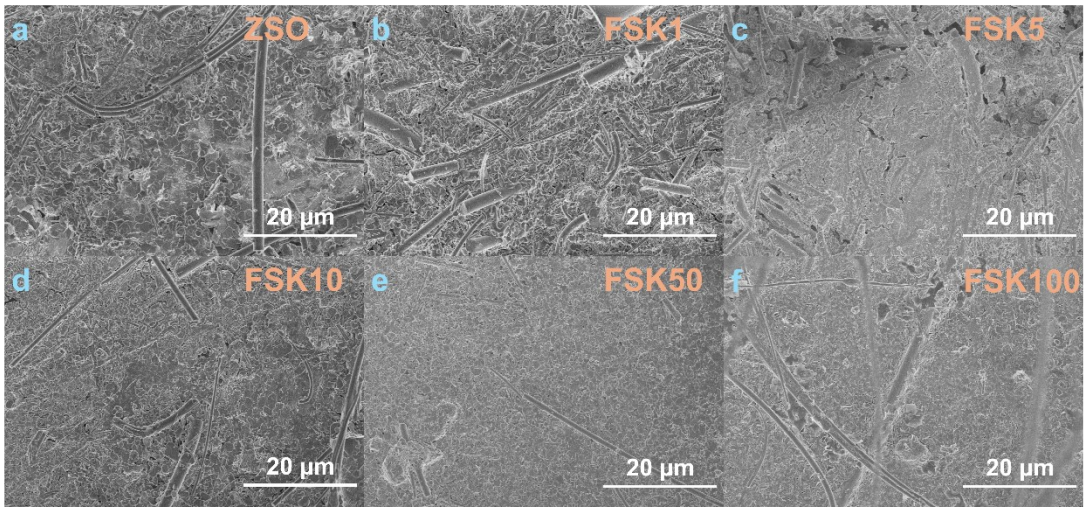

Figure S15. SEM image of Zn||Zn symmetric cells with (a) ZSO, (b)FSK1, (c) FSK5, (d) FSK10, (e) FSK50 and (f) FSK100 after 50 cycles at 1 mA cm^{-2} and 1 mAh cm^{-2}

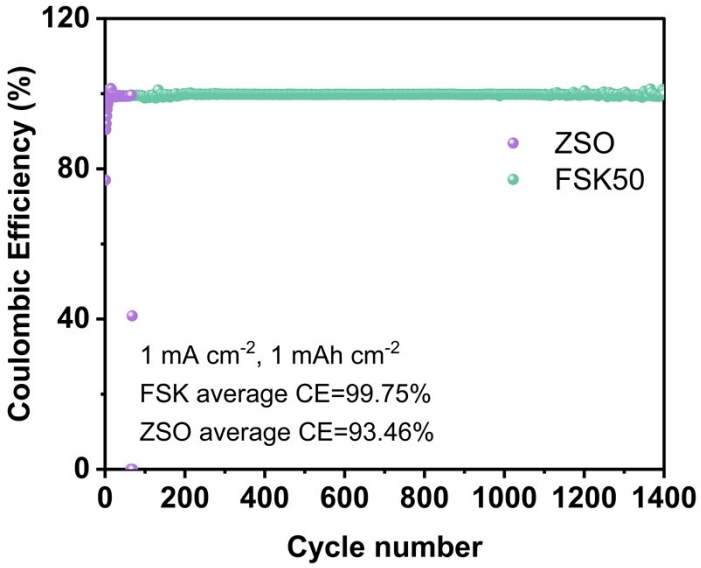

Figure S16. Coulombic efficiency of different cells at 1 mA cm^{-2} and 1 mAh cm^{-2}.

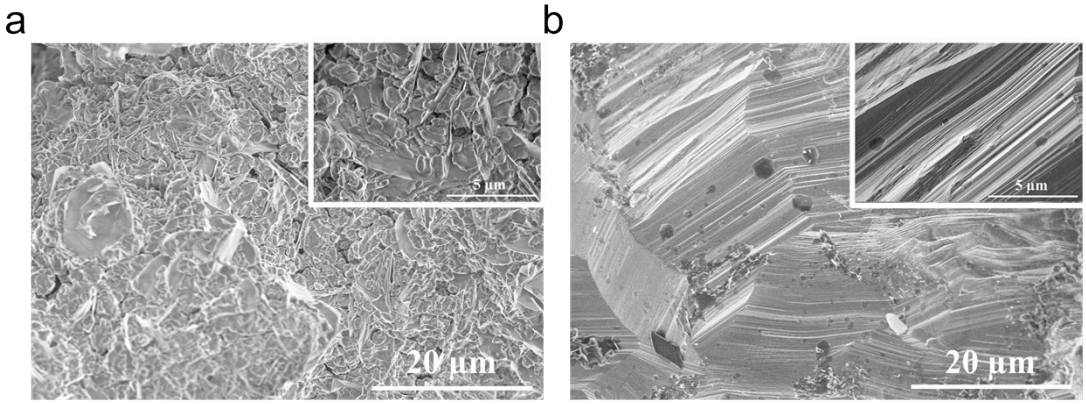

Figure S17. SEM images of Zn plating at 5 mA cm^{-2} and 10 mAh cm^{-2} on the surfaces of (a) ZSO and (b) FSK50.

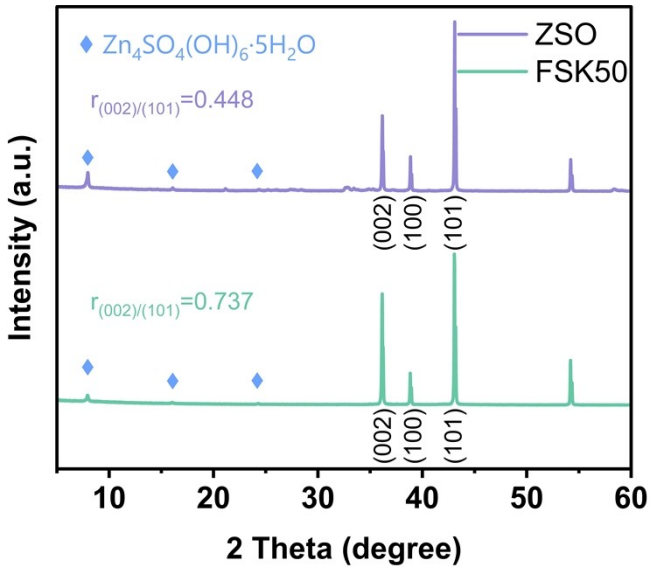

Figure S18. XRD patterns of different Zn electrodes after Zn plating at 5 mA cm^{-2} and 10 mAh cm^{-2} in ZSO and FSK50, respectively.

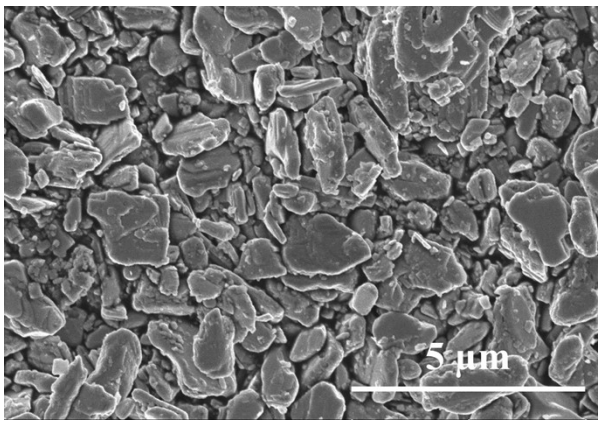

Figure S19. SEM image of V_2O_5 powder.

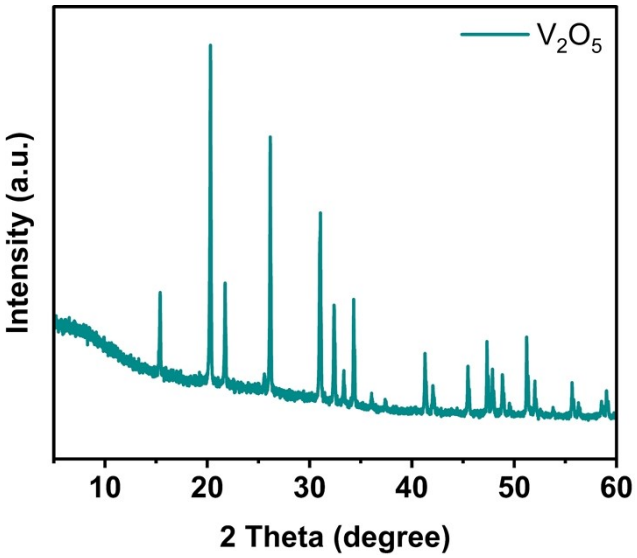

Figure S20. XRD pattern of V_2O_5 powder.

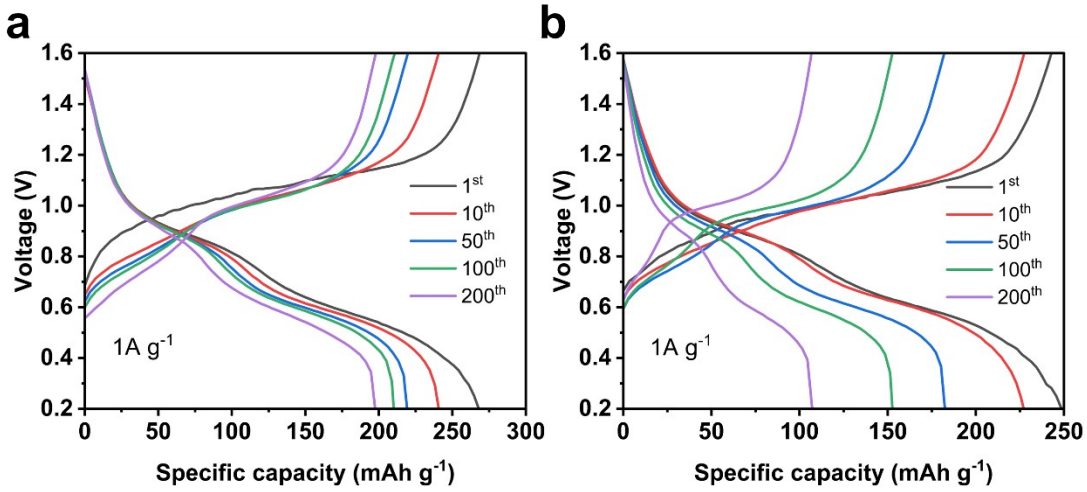

Figure S21. GCD curve of (a) cell with FSK50 and (b) cell with ZSO.

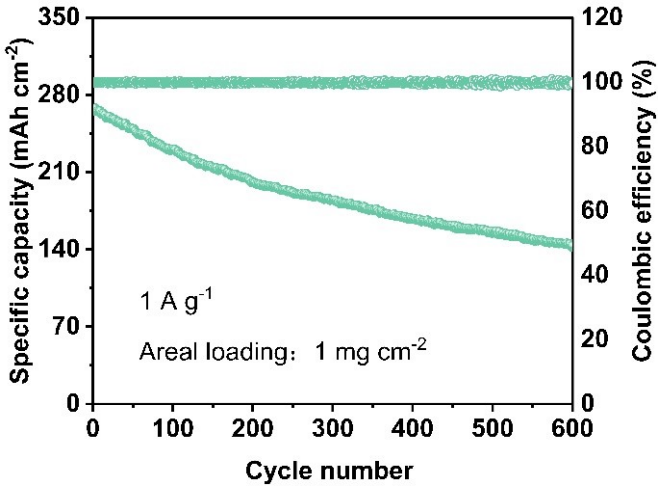

Figure S22. Long-term cycling performanceof Zn||V_2O_5 full cells with FSK50 after standing for 7 days.

Table S1. Performance comparison of this work with other previous reports.

Modification strategies	Current density (mA cm^{-2}), Areal capacity (mAh cm^{-2})	Cycle life (h)	Ref.
CH@AGM	**1, 1**	**110**	[1]
Carboxymethyl cellulose	**1, 1**	**1050**	[2]
β-CD	**5, 5**	**350**	[3]
TBA_2SO_4	**10, 2**	**400**	[4]
ZF@F-TiO_2	**1, 1**	**460**	[5]
Trehalose	**5, 2.5**	**200**	[6]
Saccharin	**10, 10**	**550**	[7]
Sodium citrate	**5, 2**	**850**	[8]
Ammonium succinate (AS)	**10, 2**	**1230**	[9]
Zn@KL	**4.4, 1.1**	**800**	[10]
DMSO	**0.5, 0.5**	**1000**	[11]
Locust bean gum (LBG)	**2, 2**	**1160**	[12]
Zn@ZnS	**2, 2**	**1125**	[13]
EG	**2, 1**	**140**	[14]
FSK	**1, 1** **10, 1**	**1500** **1200**	**This work**

Reference

1. J. Zhi, S. Li, M Han and P Chen, Biomolecule-guided cation regulation for dendrite-free metal anodes, *Sci. Adv.*, 2020, **6(32)**, eabb1342.
2. Y. Xiong, Q. Li, K. Luo, L. Zhong, G. Li, S. Zhong and D. Yan, Low cost carboxymethyl cellulose additive toward stable zinc anodes in aqueous zinc ion battery, *J. Energy Storage*, 2023, **68**, 107655.
3. M. Qiu, P. Sun, Y. Wang, L. Ma, C. Zhi and W. Mai, Anion-Trap Engineering toward Remarkable Crystallographic Reorientation and Efficient Cation Migration of Zn Ion Batteries, *Angew. Chem. Int. Ed.*, 2022, **61**, e202210979.
4. A. Bayaguud, X. Luo, Y. Fu and C. Zhu, Cationic Surfactant-Type Electrolyte Additive Enables Three-Dimensional Dendrite-Free Zinc Anode for Stable Zinc-Ion Batteries, *ACS Energy Lett.*, 2020, **5**, 3012-3020.
5. Q. Zhang, J. Luan, X. Huang, Q. Wang, D. Sun, Y. Tang, X. Ji and H. Wang, Revealing the role of crystal orientation of protective layers for stable zinc anode, *Nat. Commun.*, 2020, **11**, 3961.
6. D. Liu, X. Song, Z. Liu, L. Cheng and Z. Jiang, Heteroatom-free cyclic ether enables synergistic

optimization of solvation and hydrogen-bonding in aqueous zinc batteries, *J. Colloid Interface Sci.*, 2026, **706**, 139766.
7. C. Huang, X. Zhao, S. Liu, Y. Hao, Q. Tang, A. Hu, Z. Liu and X. Chen, Stabilizing Zinc Anodes by Regulating the Electrical Double Layer with Saccharin Anions, *Adv. Mater.*, 2021, **33**, 2100445.
8. X. Liu, L. Yue, W. Dong, Y. Qu, X. Sun and L. Chen, Sodium Citrate Electrolyte Additive to Improve Zinc Anode Behavior in Aqueous Zinc-Ion Batteries, *Batteries*, 2024, **10**, 97.
9. X. Fan, L. Chen, Y. Wang, X. Xu, X. Jiao, P. Zhou, Y. Liu, Z. Song and J. Zhou, Selection of Negative Charged Acidic Polar Additives to Regulate Electric Double Layer for Stable Zinc Ion Battery, *Nano-Micro Lett.*, 2024, **16**, 270.
10. C. Deng, X. Xie, J. Han, Y. Tang, J. Gao, C. Liu, X. Shi, J. Zhou and S. Liang, A Sieve-Functional and Uniform-Porous Kaolin Layer toward Stable Zinc Metal Anode, *Adv. Funct. Mater.*, 2020, **30**, 2000599.
11. L. Cao, D. Li, E. Hu, J. Xu, T. Deng, L. Ma, Y. Wang, X.-Q. Yang and C. Wang, Solvation Structure Design for Aqueous Zn Metal Batteries, *J. Am. Chem. Soc.*, 2020, **142**, 21404-21409.
12. K. Wang, H. Zhan, W. Su, X.-X. Liu and X. Sun, Ordered interface regulation at Zn electrodes induced by trace gum additives for high-performance aqueous batteries, *Energy Environ. Sci.*, 2025, **18**, 1398-1407.
13. J. Hao, B. Li, X. Li, X. Zeng, S. Zhang, F. Yang, S. Liu, D. Li, C. Wu and Z. Guo, An In-Depth Study of Zn Metal Surface Chemistry for Advanced Aqueous Zn-Ion Batteries, *Adv. Mater.*, 2020, **32**, 2003021.
14. R. Qin, Y. Wang, M. Zhang, Y. Wang, S. Ding, A. Song, H. Yi, L. Yang, Y. Song, Y. Cui, J. Liu, Z. Wang, S. Li, Q. Zhao and F. Pan, Tuning Zn^{2+} coordination environment to suppress dendrite formation for high-performance Zn-ion batteries, *Nano Energy*, 2021, **80**, 105478.